JOURNAL OF OPTOELECTRONICS AND ADVANCED MATERIALS Vol. 9, No. 3, March 2007, p. 512 - 521

Invited Lecture

Calcium oxalates and prehistoric paintings. The usefulness of these biomaterials

A. HERNANZ*, J. M. GAVIRA-VALLEJO, J. F. RUIZ-LÓPEZ[a]
Departamento de Ciencias y Técnicas Fisicoquímicas, Facultad de Ciencias, Universidad Nacional de Educación a Distancia (UNED), Senda del Rey, 9, E-28040 Madrid, Spain
[a]*Departamento de Prehistoria y Arqueología, Facultad de Geografía e Historia, UNED, Senda del Rey, 7, E-28040 Madrid, Spain*

Oxalate accretions of whewellite ($CaC_2O_4.H_2O$) and weddellite ($CaC_2O_4.(2+x)H_2O$, $x \leq 0.5$) have been found by Raman microscopy on Post-Palaeolithic rock paintings from open-air rock shelters of Triassic sandstone in the Sierra de las Cuerdas (Cuenca, Spain). Scanning electron microscopy (SEM) of these accretions suggests that they could have been produced by colonies of lichens that lived on the rock surface. Raman and petrologic microscopy of samples from a painting panel has revealed the nature and distribution of the components: α-quartz, haematite, whewellite, gypsum, muscovite, microcline, anatase and rutile. Energy-dispersive X-ray (EDX) spectroscopy confirms these results. The observed microstratigraphic oxalate layers are very helpful for archaeological studies. The pigment, haematite, is located between two of them and some superimposition of pictographs or repainting processes have been detected. The observed oxalate layers protect these works of art, prevent weathering and have been used for the first AMS ^{14}C dating of Post-Palaeolithic rock art in Spain.

(Received November 15, 2006; accepted December 21, 2006)

Keywords: Whewellite, Weddellite, Prehistoric paintings, Raman microscopy, SEM/EDX

1. Introduction

The minerals whewellite [$CaC_2O_4.H_2O$], weddellite [$CaC_2O_4.(2+x)H_2O$, $x \leq 0.5$] and caoxite [$CaC_2O_4).3H_2O$] are known as calcium oxalate hydrated minerals. Whewellite and caoxite have crystal structures consisting of sheets of Ca^{2+} and oxalate ions although weddellite is composed of chains leaving pores among them. Up to 0.5 moles of zeolitic water per mole of oxalate may be located in these pores. Sheets of caoxite are corrugated by hydrogen bonds but whewellite has flat sheets [1-3]. Whewellite is more stable than weddellite, the monohydrated form being stable up to around 434K, above which temperature anhydrous calcium oxalate is formed. At 752K, the oxalate transforms into calcium carbonate with loss of carbon dioxide [4]. The actual dehydration process of caoxite was characterized by direct transformation into whewellite at 389.5 K not via weddellite [3].

Calcium oxalates are commonly associated with diseases or deterioration. They are toxic end products of metabolism in man and animals which cause urinary deposits (urolithiasis) [5]. Many fungi and lichens produce these compounds [6-11], consequently their presence in works of art is considered a sign of biodeterioration [12-14]. However, instead of a problem, calcium oxalates may be considered for their usefulness and biological role. The stability against environmental agents and the very low solubility product of the monohydrate, $K_{sp} = 2.0 \times 10^{-9}$ mol^2dm^{-6} at 25 °C [15], makes whewellite useful for protecting limestone surfaces of buildings and monuments against weathering [16-18]. Calcium oxalates are essential for some organisms, and their crystals are very often found in plant tissues [19-22]. They are generally formed inside plant cells and may have various functions. They act as water regulators in lichens [23]. They could contribute towards keeping up an ionic equilibrium, and towards regulating the osmotic pressure. The formation of crystals could control toxic concentrations of oxalic acid and calcium inside the cells. From another point of view, calcium oxalates could be considered as storage products, containing essential ions for plants [19,22].

Calcium oxalates may be detected by infrared and Raman spectroscopy. Nevertheless, the most common oxalates, whewellite and weddellite, are easier to distinguish in the Raman spectra [5]. Raman microscopy is particularly useful for *in situ* detection of oxalates in organic tissues [24]. Frost et al. [25,26] have published a collection of Raman spectra of natural oxalates.

An extensive study of prehistoric paintings in the Sierra de las Cuerdas (Cuenca, Spain) has been accomplished by our group. About one thousand figures of Post-Palaeolithic rock art have been discovered up to the present in more than forty rock shelters. Most of them were included in the UNESCO World Heritage List in 1998. They are made on reddish Triassic sandstone (Buntsandstein facies). The chemical and mineralogical composition of the pigments used, substrata, accretions and alterations have been investigated. The painting panel 2 in the Cueva del Tío Modesto is particularly interesting

as motifs of different styles are represented and several phases of accretion may be differentiated [27-29], Fig. 1. Traces of whewellite and weddellite were detected in previous analyses of a sample of pigment from a selected pictograph of this panel [27], and whewellite is the main component of the blue-greyish accretion that spreads across the whole panel [28]. This type of accretion or patina is very often found covering sandstone surfaces in the region. Therefore, we wonder whether these oxalates could give information on the paintings. Is there any relationship or stratigraphic order between substratum, pigment and accretions? And finally, could information on the origin of these oxalates be obtained? In this work we try to find answers to these questions.

The study of calcium oxalate crusts on exposed rock surfaces gives significant information on palaeoclimate reconstructions [30]. Previous work on oxalates and prehistoric paintings has been carried out [31,32]. Oxalates have been used for dating [33] and some ^{14}C AMS dating of prehistoric paintings has been performed from oxalate crusts [34,35]. Raman microscopy, scanning electron microscopy, SEM, and energy dispersed X-ray spectroscopy, EDX, are techniques specially helpful in determining the composition and microscopic structures of prehistoric paintings [27,36-40].

Samples of accretions from panel 2 of the Cueva del Tío Modesto have been studied by Raman microscopy, SEM and EDX techniques. The microstratigraphy of a thin section of a flake of pigment from a significant pictograph has been observed with a petrologic microscope using polarized light, Fig. 2. The nature of the observed microcrystals has been determined by Raman microscopy.

Fig. 1. Central part of the painting panel 2 at Cueva del Tío Modesto (Henarejos, Cuenca). The black arrow, on the left of the photograph, shows the place where a pigment sample of the deer 47 (15-CTM:047) has been collected. The reddish sandstone substratum, the blue-greyish crust and the deterioration of the panel due to a flaking effect [28] are evident.

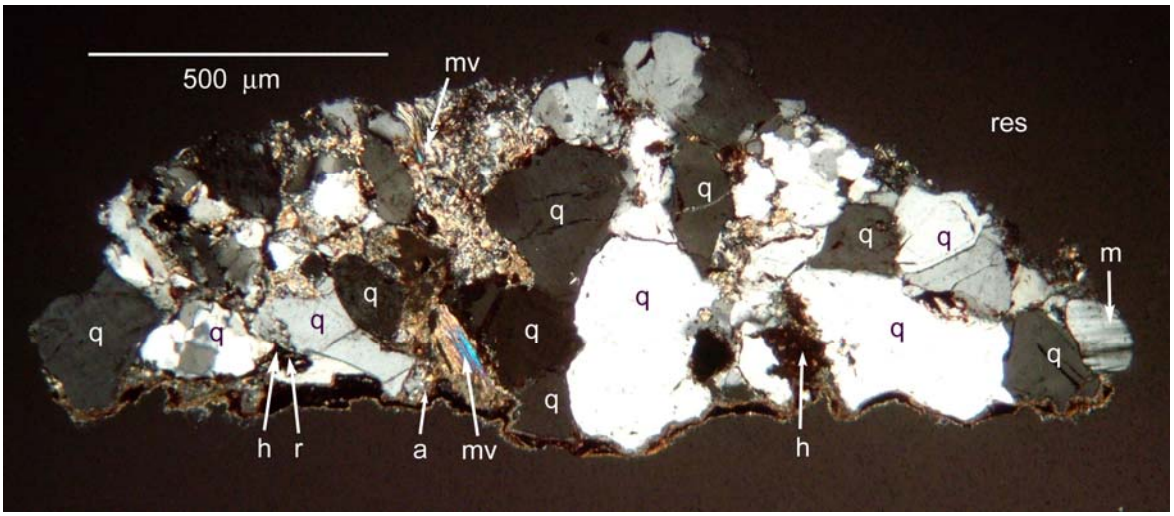

Fig. 2. Microphotograph with polarized light of a polished thin section (20 µm) of a small flake from the sample 15-CTM:047 (deer 47). Microcrystals of the substratum of the pictograph (Buntsandstein Triassic sandstone) were identified by Raman microscopy (Fig. 4): (q) α-quartz, (m) microcline, (h) haematite, (mv) muscovite, (a) anatase and (r) rutile. α-Quartz microcrystals exhibit different colours due to different orientations of their crystallographic axes with respect to the polarized light. The sample is surrounded by polyester resin (res). The section of the external face of the flake, at the bottom of the figure, shows a layer of red pigment.

2. Experimental

An established protocol for sampling prehistoric paintings was followed [27,28,41]. The samples were numbered according to a code developed for the Micr-Art database [28,41]. Microphotography of significant parts of the painting panel by *in situ* optical microscopy helped to decide the sampling points. Samples of accretions (14-CTM:sus, 23-CTM:alt and 80-CTM:alt) and a small flake of pigment (15-CTM:047) from a zoomorphic motif (deer 47), Fig. 1, were extracted. Extreme care was taken to avoid sample contamination: samples were collected and handled wearing latex disposable gloves, hygienic masks and using sterile surgical blades. A new surgical blade was used for each sample. They were removed minimizing the effect on the pictographs. Macro- and microphotographs of the sampled areas were taken before and after sampling. The samples were stored in ependorf tubes.

A polished thin section (thickness 20 μm) of a flake of pigment from the sample 15-CTM:047 (deer 47) was prepared using a matrix of polyester resin. This thin section was examined with a petrologic microscope using polarized light and relevant microphotographs have been taken.

Raman spectra of the micro-crystals observed in the samples were obtained using a Jobin Yvon LabRam-IR HR-800 spectrograph according to the procedure described elsewhere [27,28,41]. The line at 632.8 nm of a He/Ne laser was used for Raman excitation. An effective power of 274 μW was measured at the sample position using a 100x objective. That is, it was kept rather below 700 μW, to avoid sample degradation [42,43]. The average spectral resolution in the Raman shift range of 100-1700 cm^{-1} was 1 cm^{-1} (focal length 800 mm, grating 1800 grooves/mm, and confocal pinhole 100 μm). The sample spot size was ~1 μm, in accordance with the 100x objective employed. An integration time between 5 and 20 s and up to 25 accumulations were used to get acceptable S/N ratios. A wavenumber shift calibration with 4-acetamidophenol and sulphur [44] in the range 150-3100 cm^{-1} using the same recording conditions gave a mean deviation of $\Delta\nu_{cal}-\Delta\nu_{obs}$ = 0.50 ± 0.16 cm^{-1} ($t_{Student}$ 95%). No manipulation (baseline adjustment, smoothing… etc.) has been applied to the spectra. The software package GRAMS/AI v.7.00 (Thermo Electron Corporation, Salem, NH, USA) was used to help with the readings of the wavenumber corresponding to the peaks.

The micromorphology and distribution of the components in the samples were determined using a Hitachi S-3000N scanning electron microscope equipped with a Everhart-Hornley detector of secondary electrons with a resolution of 3 nm. X-ray microanalysis (EDX) of the samples was carried out with an energy dispersed X-ray spectrometer Rontec Xflash Detector 3001, coupled to the scanning electron microscope, without Be window and Peltier refrigerated. The samples were previously Au/Pd coated in a Polaron Range SC7620 sputter-coater.

3. Results and discussion

Raman spectra of samples 14-CTM:sus, 23-CTM:alt and 80-CTM:alt, Fig. 3, show an intense pair of whewellite bands at 1464/1492 cm^{-1}. This doublet is assigned to the C=O symmetric stretching (ν_sC=O) mode of whewellite [5,25,26,45]. The band at 1629 cm^{-1} corresponds to the antisymmetric C=O stretching mode (ν_aC=O) and the band at 896 cm^{-1} to the νC-C mode [5,25,26]. The ν_sC=O and νC-C modes of weddellite [5,25,26,45] give rise to the bands observed at 1477 and 904 cm^{-1} respectively. The δO-C=O bending, CaO ring deformation and CaO stretching modes of these oxalates produce a band [25,46] at about 500 cm^{-1}. The bands at 194, 209 and 225 cm^{-1} are assigned to lattice modes of these oxalates [25,26]. The spectra obtained confirm previous results [28] indicating that the main component of the accretions in the painting panel 2 of the Cueva del Tío Modesto is whewellite. The very broad bands at 1332 and 1595 cm^{-1} are due to amorphous carbon. Previous studies on this panel [27,28], suggest that these bands may be due to smoke particles from fires lit in the rock shelter.

The morphology and distribution of the components of the substratum of pictograph 47 may be observed in the microphotograph of the thin section of a flake of the sample 15-CTM:047, Fig. 2. Their mineralogical composition has been determined by Raman microscopy. Representative spectra of the components of the thin section are shown in Fig. 4. The letters included on several positions of the microphotograph, Fig. 2, indicate points from which spectroscopic information has been obtained to identify the nature of the corresponding microcrystal. The dominant component of the sandstone substratum is α-quartz. Bands at 130, 208, 356 and 466 and 1160 cm^{-1} (Fig. 4C-d) appear in the spectra of the crystals of this mineral [45], that it is found all over the sample. Traces of the polyester resin used to prepare the thin section are also found in different parts of the sample. A microcline crystal, $K[AlSi_3O_8]$, has been detected, which exhibits the characteristic minute multiple twinning when illuminated with polarized light (Fig. 2, right). The typical Raman bands of this feldspar [47] are clearly identified in the spectrum (Fig. 4B), for instance, the bands observed at 272, 291, 460, 481 and 519 cm^{-1}. Some haematite, α-Fe_2O_3, particles are located in the thin section; they could be responsible for the reddish colour of this type of sandstone. An example of the spectra of these particles is given in Fig. 4A-c. It shows the haematite bands [28,36,40,42,45,48] at 231 (A_{1g}), 250 (E_g), 297 (E_g), 414(E_g), 499 (A_{1g}), 614 (E_g) and 660 cm^{-1}. The broad band at ~1320 cm^{-1} has been assigned to a two-magnon scattering of haematite [42]. The very weak bands at 1468 and 1495 cm^{-1} indicate that traces of whewellite [45] have

penetrated about 120 μm inside the substratum. Muscovite, $K\{Al_2[AlSi_3O_{10}](OH)_2\}$, a di-octahedral phyllosilicate of the micas group, is another component of the sandstone. It may be observed as groups of bluish sheets in Fig. 2. Their Raman spectra, Fig. 4C-e and Fig. 4D-i, show bands at 708 and 3627 cm^{-1} that are assigned to the SiO_4 symmetric stretching mode [49-51] and the OH stretching mode [50,51] respectively. Other bands of muscovite appear at 204, 266, 415, and 759 cm^{-1} [49-51]. Weak bands of polyester resin and whewellite are also observed in the spectrum of muscovite in a location at about 160 μm inside the substratum. The bands of gypsum [28,45,52,53] at 1008, 1141 and 3405 cm^{-1} are also detected in these spectra. These bands often appear in the spectra of sandstone flakes, and channels of gypsum filling the sandstone pores in flaking areas were observed in a previous work [28]. Finally, some small microcrystals of two forms of titanium oxide, TiO_2, have been discovered: anatase and rutile, Fig. 2. The very strong band of anatase at 144 cm^{-1}, Fig. 4A-a, and the three weak bands at 397, 516 and 638 cm^{-1} clearly identify this mineral [45,48,54-56]. However, rutile shows two weak bands at 147 and 242 cm^{-1}, Fig. 4A-b, and two strong bands at 450 and 615 cm^{-1} [45,48,55,56]. Some of these minerals detected in the substratum of the paintings were previously considered characteristic of Triassic sandstone (Upper Buntsandstein facies) from the Southern Iberian Range [57,58].

The microstratigraphy of the external face of the flake of pigment from pictograph 47 (sample 15-CTM:047), may be observed in the microphotographs of Fig. 5. The pigment used by the prehistoric artists was haematite, Fig. 6. It forms a red layer recognizable in the microphotograph Fig. 5A. No other mineral, iron oxide, oxyhydroxide (magnetite, maghemite, goethite, lepidocrite…) [42] has been detected in this layer. Aside from haematite bands, only weak spectral features from traces of whewellite and weddellite are observed. No organic compound acting as binder has been detected. Therefore, the artists used a very pure pigment with no binders, or they disappear after thousands of years [28,40]. The pigment layer is bracketed or encapsulated between adjacent natural oxalate layers of whewellite, Fig. 5A and Fig. 6. This was observed in other prehistoric paintings [32]. Whewellite and weddellite are present in sample 15-CTM:047 (deer 47) [28]. However, in some parts of the external face of the flake, two pigment layers separated by an oxalate layer may be observed, Fig. 5B. Superimpositions of different pictographs, something common in this panel, or repainting processes would have resulted in this microstratigraphy [59]. Three samples of oxalate accretions from this panel have been used for the first AMS ^{14}C dating of oxalate crusts related to Spanish prehistoric rock art [29]. The pigment cannot be dated directly by this technique. Even so, as it is bracketed between oxalate layers of similar thickness, the results obtained could be an approximation to the age of the paintings.

Some gypsum crystals are observed on the surface of the panel, Figs. 5 and 6. This is a frequent finding in sandstone surfaces suffering the flaking effect [60]. Gypsum is the dominant salt in the weathering process of Triassic sandstone (Buntsandstein facies) [28,58], and gypsum channels have been discovered in sandstone pores, rising the surface in flaking areas of panel 2 [28].

According to the results indicated before and those obtained in a previous study [28], the blue-greyish crust that extends over panel 2 is composed mainly of whewellite, some parts resulting from gypsum efflorescence and traces of weddellite. SEM microphotographs of the external surface of this crust (samples 14-CTM:sus and 23-CTM:alt), Fig. 7, reveal protuberances and microstructures similar to those observed in whewellite-rich crusts produced by lichens [30]. Whewellite crystals are usually very small. It is difficult to observe large crystals of this monohydrate due to its very low solubility product [61]. An accumulation of whewellite microcrystals may be compared with gypsum crystals in Fig. 7D. On the other hand, whewellite crystallises in a monoclinic leaf shape, Fig. 7F. Occasionally, the monohydrate precipitates as an oval shape or elongated oval shape. A crystal of these characteristics may be observed in Fig. 7F.

EDX spectra, Fig. 8, of different microscopic areas of the external face of the blue-greyish crust confirm the composition previously determined by vibrational spectroscopy. The EDX spectrum, Fig. 8A, of the entire area corresponding to the microphotograph of Fig. 7A shows significant O, Ca and C peaks from whewellite and Si, Al, Mg and K peaks from the sandstone substratum (α-quartz, microcline, muscovite, traces of haematite and of other possible clay minerals). The Pd/Au coating of the samples was essential to reach an appropriate contrast in the SEM microphotographs. Consequently, it produces Pd and Au peaks in the EDX spectra that are not considered here. The spectrum, Fig. 8B, of the accumulation of microcrystals in Fig. 7D(w) is similar to the spectrum described above, Fig. 8A, i.e. these are whewellite microcrystals on a sandstone substratum. A representative spectrum of the large crystals, Fig. 7D(g), surrounding this accumulation is shown in Fig. 8C. Strong S, Ca and O peaks confirm the presence of gypsum in different locations on the painting panel.

Finally, an additional sample extracted from the left of this panel (80-CTM:alt) has been observed by SEM, Fig. 9. The Raman spectra of the external surface of this

sample, Fig. 3B-a, and the SEM microphotograph shown in Fig. 9, reveal the presence of fungal hyphae encrusted with small crystals of whewellite.

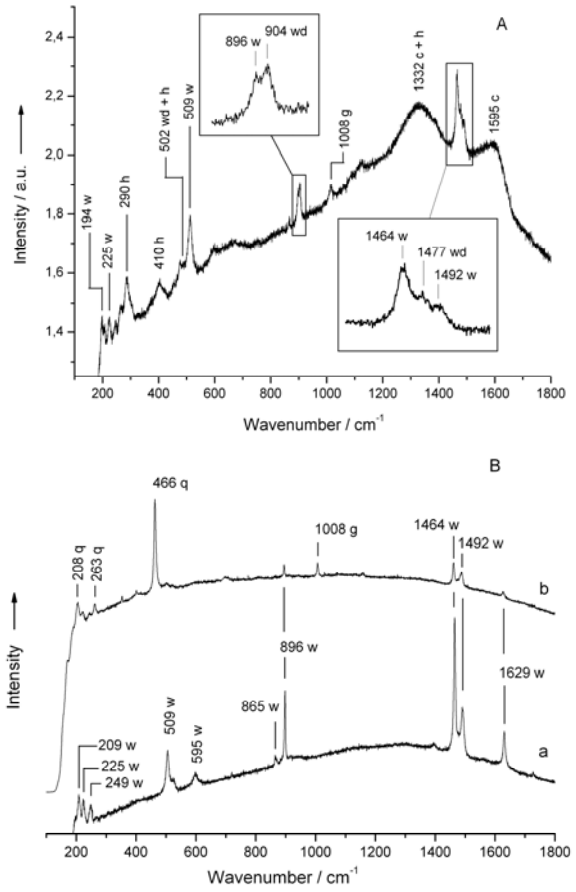

Fig. 3. A: Raman spectrum obtained from the sample 14-CTM:sus; w, whewellite; wd, weddellite; c, amorphous carbon; g, gypsum; h, hematite. B: Raman spectra obtained from the samples (a) 80-CTM:alt and (b) 23-CTM:alt; q, α-quartz.

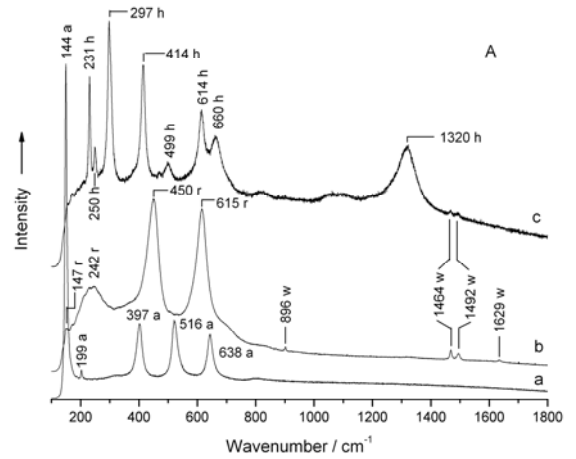

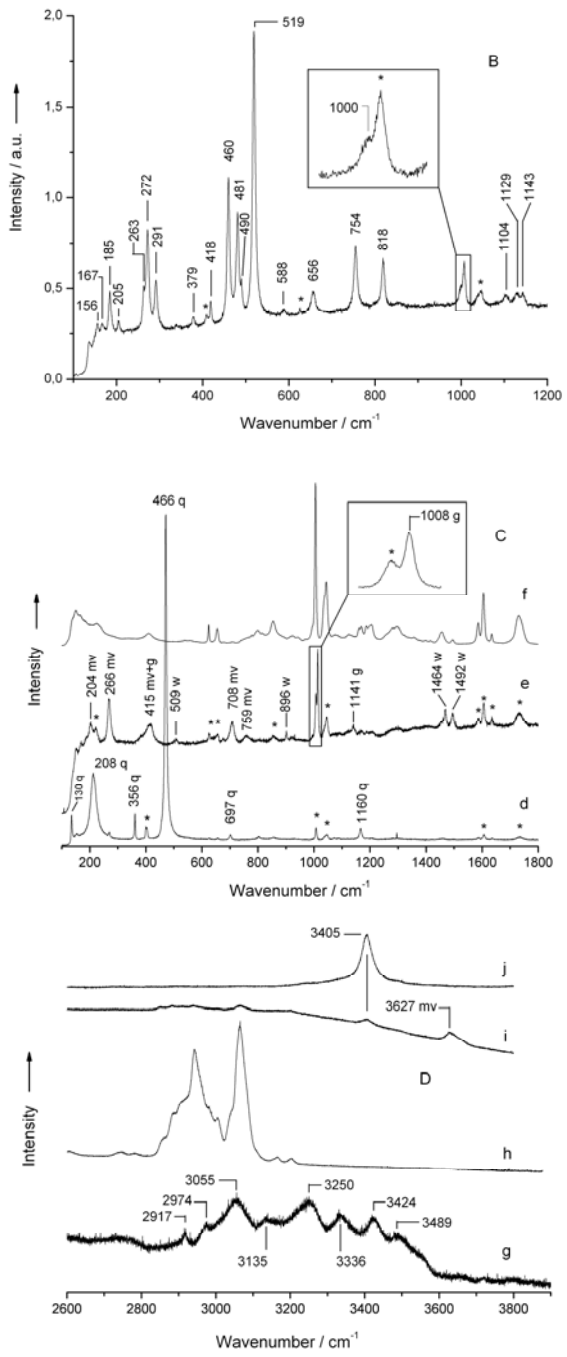

Fig. 4. Raman spectra of components of the substratum of pictograph 47 corresponding to the sample 15-CTM:047, see Fig. 2. A: (a) anatase, a; (b) rutile, r, with traces of whewellite, w; (c) haematite, h, with traces of whewellite. B: microcline with traces of polyester resin. C: (d) α-quartz, q, with traces of polyester resin; (e) muscovite, mv, with gypsum, g, and traces of whewellite and polyester resin; (f) polyester resin. D: (g) whewellite; (h) polyester resin; (i) muscovite, mv, with gypsum and traces of whewellite and polyester resin; (j) gypsum. (*) Bands due to remains of the polyester resin used to prepare the polished thin section.

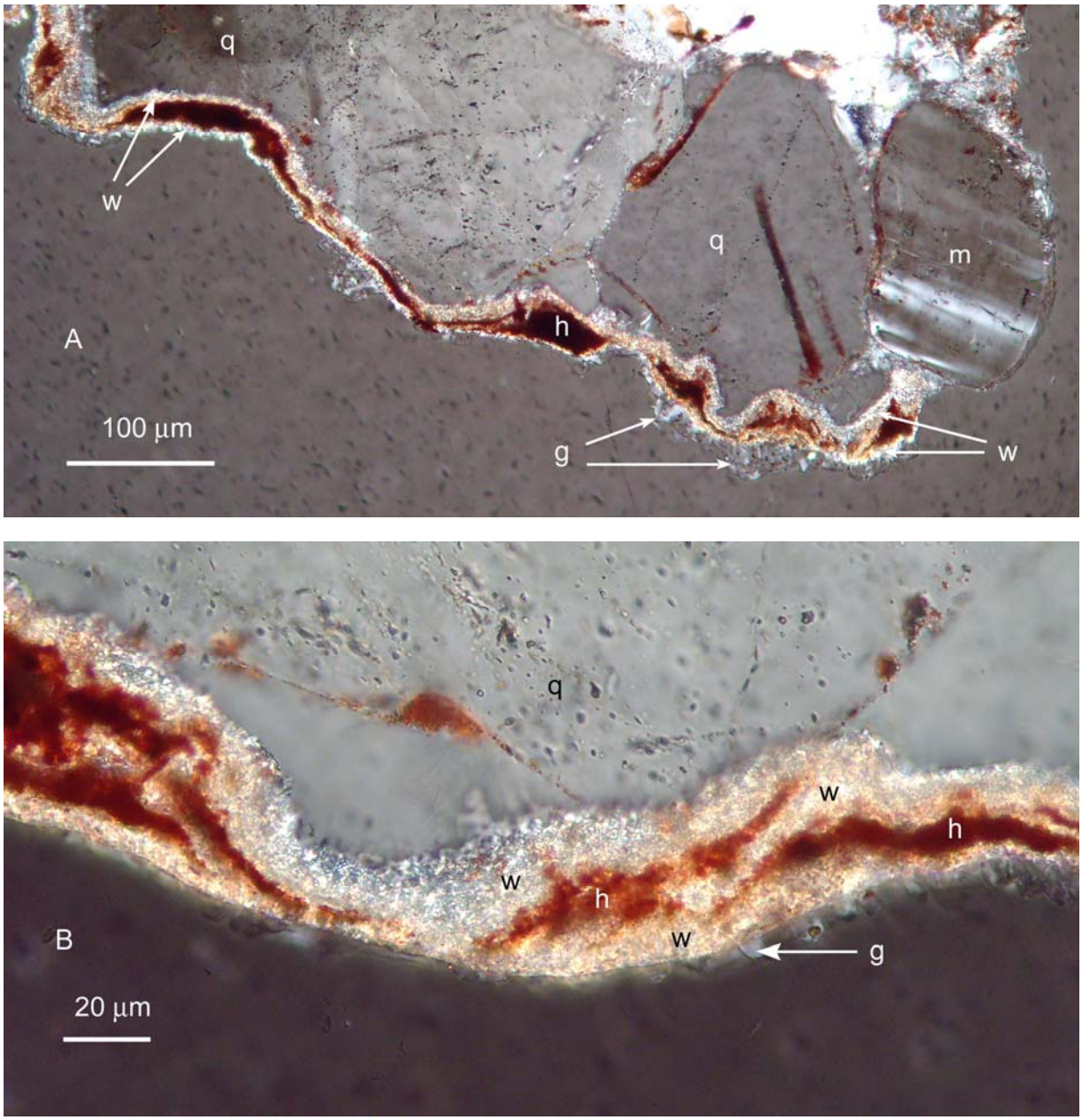

Fig. 5. Microphotographs with polarized light of the section of the pigment layer of pictograph 47 (15-CTM:047). Magnified views of Fig. 2. (A) The layer of red pigment appears between layers of white oxalate micro-crystals at the bottom of the image. Microphotograph (B) reveals two pigment layers. The composition of the observed layers (Fig. 6) and substratum was identified by Raman microscopy: (w) whewellite, (h) haematite, (g) gypsum, (q) α-quartz and (m) microcline.

4. Conclusions

Considering the results obtained by Raman microscopy and SEM/EDX techniques in this work, as well as previous results from the paintings of Cueva del Tío Modesto shelter [27,28], from other archaeological sites [30-35], and the production of oxalates by lichens [6-11], it is suggested that the blue-greyish crust of the painting panel 2 is the result of the activity of lichens that live or have lived on the surface of the rock used by the prehistoric painters. The presence of whewellite up to 160 µm inside the substratum is a sign of the fungal hyphae activity inside the sandstone.

Whewellite is dominant in very old calcium oxalate accretions. Traces of weddellite are also observed. They are found more often in the spectra of lichens [6]. The monohydrate appears as the more stable form. The discovered oxalate accretions have made possible the first AMS ^{14}C dating of Post-Palaeolithic rock art in Spain. These accretions have resisted weathering during thousands of years, as well as the action of oxalate degrading bacteria that oxidize calcium oxalate into

calcium carbonate [62,63]. Hence, layers of calcium oxalates operate as protecting agents on the prehistoric paintings. This is important information for conservators. They should avoid the removal of these layers that have protected the paintings in open air rock shelters during thousands of years.

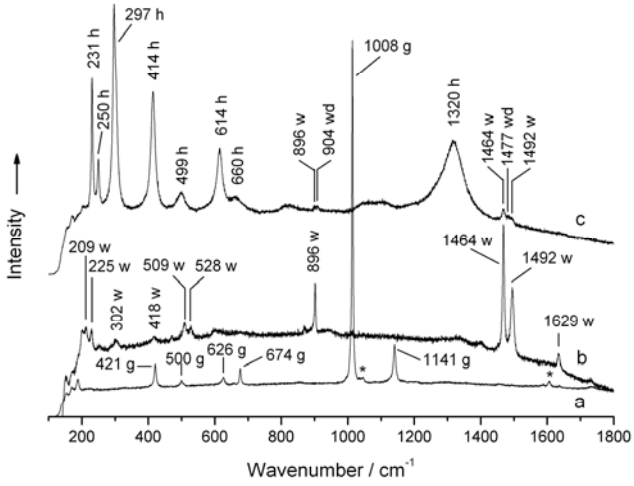

Fig. 6. Raman spectra of representative points in the external layers of pictograph 47 (15-CTM:047), see Fig. 5: (a) gypsum, g; (b) whewellite, w; (c) haematite, h, with traces of whewellite and weddellite, wd. (*) Bands due to remains of the polyester resin used to prepare the polished thin section.

The composition of the substratum of the paintings, Triassic sandstone (Upper Buntsandstein facies), has been determined: α-quartz, microcline, muscovite, haematite, and traces of anatase and rutile. The microstratigraphy of a significant pictograph have revealed that very pure haematite was used as pigment. No binders have been detected. The pigment layer appears bracketed between adjacent whewellite layers. Some superimpositions of pictographs or repainting processes have been observed. Gypsum crystals have been detected in some parts of the surface of the painting panel, especially those suffering from sandstone flaking, a weathering process due to gypsum efflorescence [28,58,60].

According to the microstratigraphic study, a time sequence of events on the rock surface of the panel could be suggested. An initial lichen colonisation of the sandstone surface left the innermost oxalate layer. Then the prehistoric artists found an area of the widespread reddish sandstone coated with a blue-greyish patina, and thus especially appropriate to use a red pigment. The pictographs were covered by a second oxalate layer produced by a new lichen colonisation. Possible repaints or superposition of pictographs on this new oxalate layer were also covered by oxalates due to continued lichen activity. Finally, crystallization of gypsum on the sandstone pores approaching the surface left gypsum crystals on some locations and provoked the flaking process that the painting panel is suffering from.

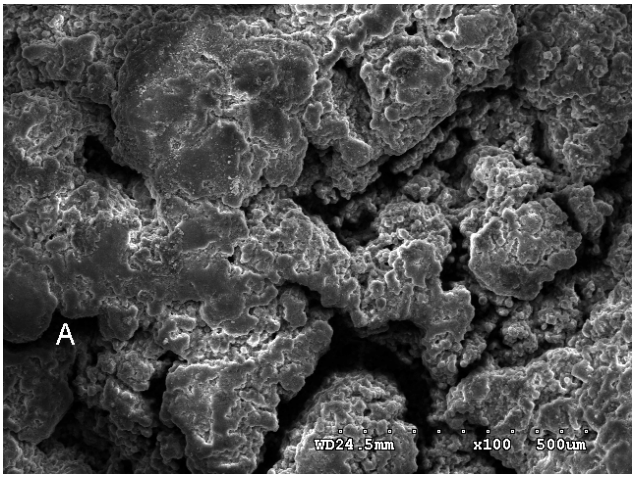

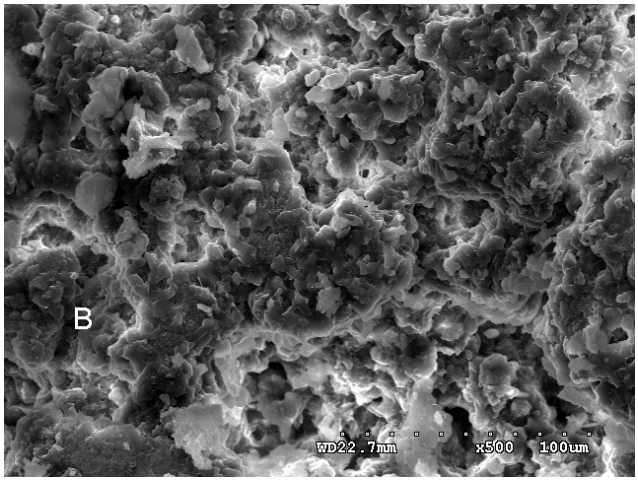

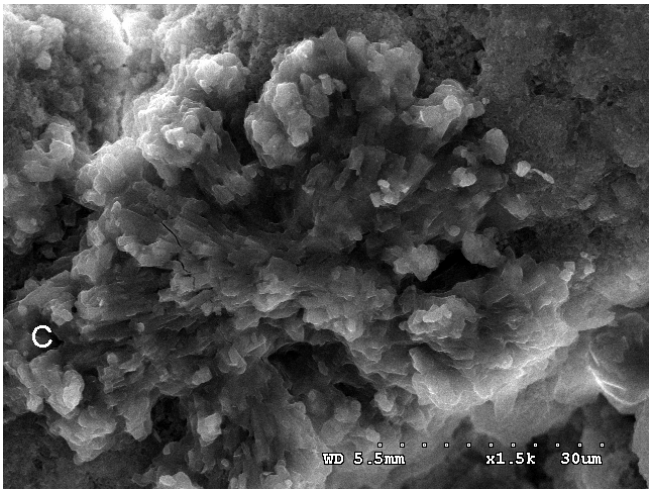

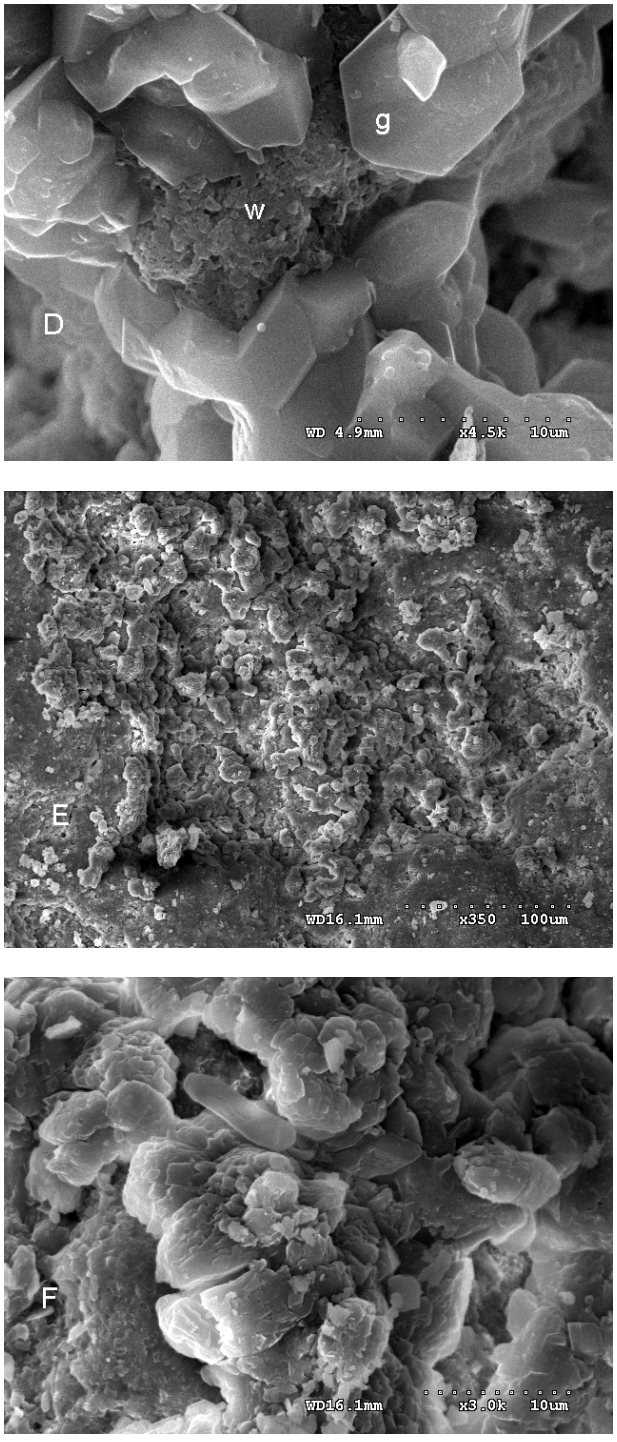

Fig. 7. SEM microphotographs of the blue-greyish crust observed on panel 2. Sample 14-CTM:sus: (A) whewellite-rich protuberances (dotted segment 500 μm); (B) and (C) views showing typical microstructures (dotted segment 100 and 30 μm respectively); (D) magnified view showing an accumulation of whewellite microcrystals (w) surrounded by gypsum (g) crystals (dotted segment 10 μm). Sample 23-CTM:alt: (E) whewellite-rich protuberances (dotted segment 100 μm); (F) magnified view showing an elongated oval shape microcrystal of whewellite (dotted segment 10 μm).

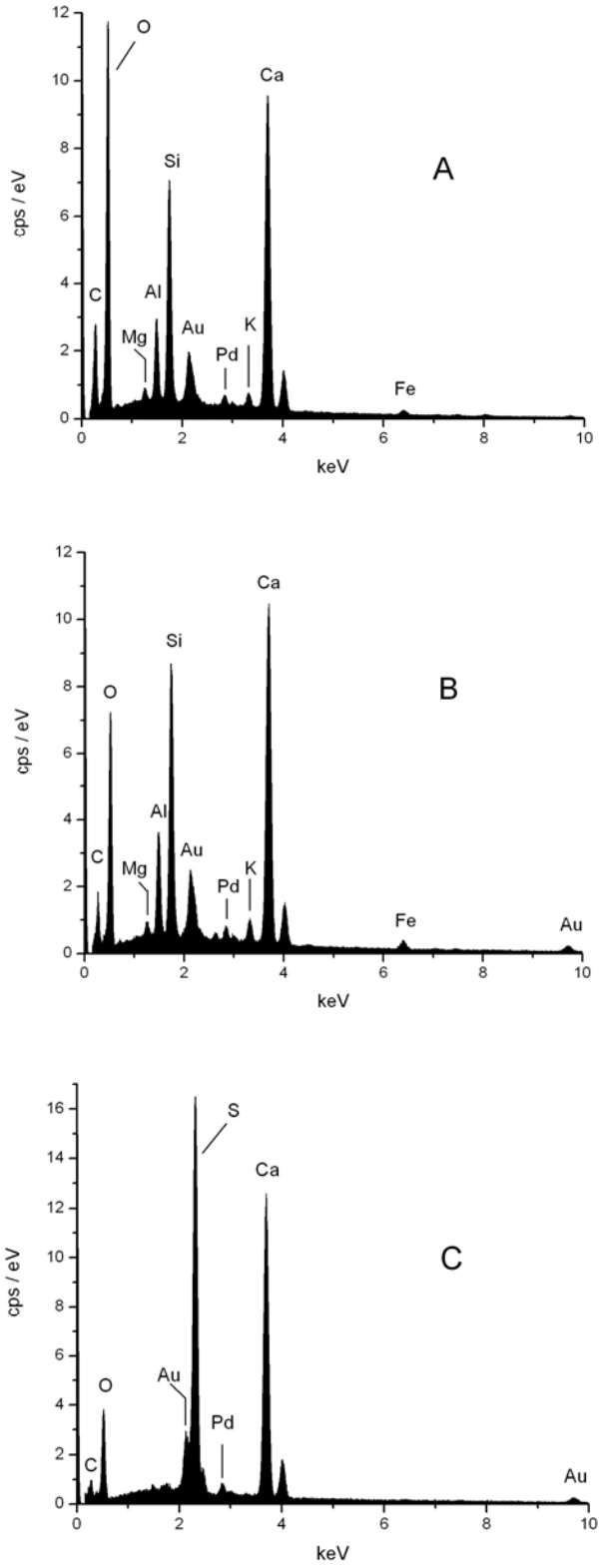

Fig. 8. EDX spectra of different microscopic areas of the external face of the blue-greyish crust from panel 2 (sample 14-CTM:sus): (A) whole area shown in Fig. 7A; (B) area of microcrystals (w) in Fig. 7D; (C) a point of the crystal (g) in Fig. 7D.

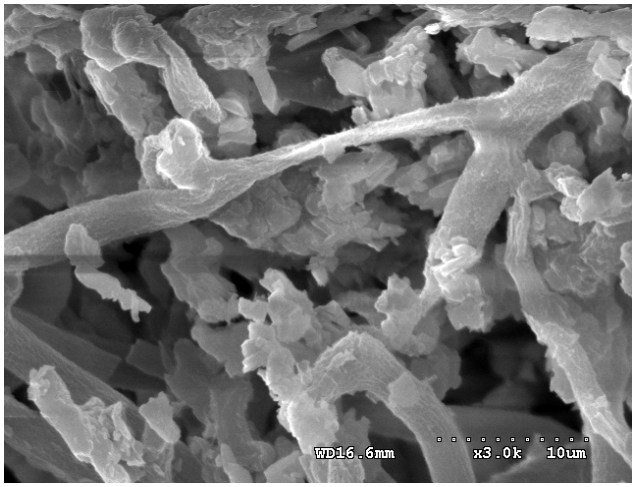

Fig. 9. SEM microphotograph showing the surface of a white alteration (sample 80-CTM:alt) observed on the left of panel 2. Fungal hyphae encrusted with small calcium oxalate crystals are observed (dotted segment 10 μm).

Acknowledgements

The authors thank S. Martín (Dept. Física Matemática y Fluidos, UNED) and Dr. E. V. Gavrilenko (Dept. Ciencias Analíticas, UNED) for assistance with SEM/EDX analyses and microscopic polarized light images, respectively. We gratefully acknowledge financial support from the Vicerrectorado de Investigación of UNED and the European Regional Development Fund (ERDF). We also thank the Consejería de Cultura de la Junta de Comunidades de Castilla La Mancha for financial support and permission to take photographs and samples of the paintings and substrata of the archaeological site. This work was supported by the Ministerio de Educación y Ciencia, I+D project CTQ2005-08959/BQU.

References

[1] V. Tazzoli, C. Domeneghetti, Am. Mineral. **65**, 327 (1980).
[2] S. Deganello, A. R. Kampf, P. B. Moore, Am. Mineral. **66**, 859 (1981).
[3] T. Echigo, M. Kimata, A. Kyono, M. Shimizu, T. Hatta, Mineral. Mag. **69**, 77 (2005).
[4] R. L. Frost, M. L. Weier, Thermochim. Acta **409**, 79 (2004).
[5] P. Carmona, J. Bellanato, E. Escolar, Biospectroscopy **3**, 331 (1997).
[6] D.W. Jackson, Scanning Electron Microsc. **III**, 279 (1981).
[7] J. D. Schoknecht, H. W. Keller, Can. J. Bot. **55**, 1807 (1997).
[8] J. M. Holder, D. D. Wynn-Williams, F. Rull Perez, H. G. M. Edwards, New Phytologist **145**, 271 (2000).
[9] J. Garty, P. Kunin, J. Delarea, S. Weiner, Plant Cell Environ. **25**, 1591 (2002).
[10] H. G. M. Edwards, M. R. D. Seaward, S. J. Attwood, S. J. Little, L. F. C. de Oliveira, M. Tretiach, Analyst **128**, 1218 (2003).
[11] S. E. Jorge Villar, H. G. M. Edwards, M. R. D. Seaward, Analyst **130**, 730 (2005).
[12] M. A. de la Torre, G. Gómez-Alarcón, C. Vizcaíno, M. T. García, Biogeochemistry **19**, 129 (1993).
[13] W. E. Krumbein, Proc. 5th European Commission Conf. "Cultural Heritage Research: a Pan European Challenge", Cracow, Poland, Ed. R. Kozlowski, 2002, pp. 39-47.
[14] S. E. Jorge Villar, H. G. M. Edwards, M. R. D. Seaward, Spectrochim. Acta A **60**, 1229 (2004).
[15] G. H. Nancollas, G. L. Gardner, J. Cryst. Growth **21**, 267 (1974).
[16] T. M. Cezar, J. Conservation Mus. Stud. **4** (1988). (http//www.jcms.ucl.ac.uk)
[17] M. Pérez-Alonso, K. Castro, M. D. Rodríguez, J. M. Madariaga, Arqueología de la Arquitectura **2**, 235 (2003).
[18] M. Pérez-Alonso, I. Martinez-Arkarazo, M. Angulo, K. Castro, J. M. Madariaga, Proc. of ITECOM, European Conference on Innovative Technologies and Materials for the Protection of Cultural Heritage. Industry, Research, Education: European Acts and Perspectives, Ed. A. Moropoulou, Technical Chamber of Greece, Athens, 2005, pp. 129-143.
[19] A. Frey-Wyssling, Am. J. Bot. **68**, 130 (1981).
[20] C. J. Prychid, P. J. Rudall, Ann. Botany **84**, 725 (1999).
[21] N. L. Lersten, H. T. Horner, Am. J. Bot. **92**, 1935 (2005).
[22] M. E. Malainine, A. Dufresne, D. Dupeyre, M. R. Vignon, M. Mahrouz, Z. Naturforsch. **58c**, 812 (2003).
[23] B. M. Clark, L. L. St. Clair, N. F. Mangelson, L. B. Rees, P. G. Grant, G. S. Bench, Am. J. Bot. **88**, 1742 (2001).
[24] J. P. Pestaner, F. G. Mullick, F. B. Johnson, J. A. Centeno, Arch. Patol. Lab. Med. **120**, 537 (1996).
[25] R. L. Frost, M. L. Weier, J. Raman Spectrosc. **34**, 776 (2003).
[26] R. L. Frost, Anal. Chim. Acta **517**, 207 (2004).
[27] A. Hernanz, J. M. Gavira-Vallejo, J. F. Ruiz-López, Asian J. Phys. **15**, 187 (2006).
[28] A. Hernanz, J. M. Gavira-Vallejo, J. F. Ruiz-López, J. Raman Spectrosc., in press.
[29] J. F. Ruiz, M. Mas, A. Hernanz, M. W. Rowe, K. L. Steelman, J.M. Gavira, Int. Newslett. Rock Art (INORA), submitted.
[30] J. Russ, R. L. Palma, D. H. Loyd, T. H. Boutton, M. A. Coy, Quaternary Res. **46**, 27 (1996).
[31] A. L. Watchman, Stud. Conservation **36**, 24 (1991).
[32] J. Russ, W. D. Kaluarachchi, L. Drummond, H. G. M. Edwards, Stud. Conservation **44**, 91 (1999).
[33] A. L. Watchman, Antiquity **67**, 58 (1993).
[34] K. L. Steelman, R. Rickman, M. W. Rowe, T. W. Boutton, J. Russ, N. Guidon, ACS Symposium Series **831** (K. Jakes ed., Archaeological Chemistry), 22 (2002).

[35] A. Watchman, S. O'Connor, R. Jones, J. Archaeol. Sci. **32**, 369 (2005).
[36] D .C. Smith, M. Bouchard, M. Lorblanchet, J. Raman Spectrosc. **30**, 347 (1999).
[37] P. Hameau, V. Cruz, E. Laval, M. Menu, C. Vignaud, L'Antropologie **105**, 611 (2001).
[38] E. Chalmin, M. Menu, J. Altuna, MUNIBE **54,** 35 (2002).
[39] E. Chalmin, M. Menu, C. Vignaud, Meas. Sci. Technol. **14**, 1590 (2003).
[40] A. Hernanz, M. Mas, B. Gavilán, B. Hernández, J. Raman Spectrosc. **37**, 492 (2006).
[41] A. Hernanz, J. F. Ruiz-López, J. M. Gavira-Vallejo in V. K. Rastogi (ed.) Perspectives in Vibrational Spectroscopy, Anita Publications, New Delhi, India, 2006, in press.
[42] D. L. A. de Faria, S. Venancio Silva, M. T. de Oliveira, J. Raman Spectrosc. **28**, 873 (1997).
[43] A. R. David, H. G. M. Edwards, D. W. Farwell, D. L. A. de Faria, Archaeometry **43**, 461 (2001).
[44] ASTM Subcommittee on Raman Spectroscopy. Raman Shift Frequency Standards: McCreery Group Summary (ASTM E 1840); American Society for Testing Materials: Philadelphia, PA; http://chemistry.ohio-state.edu/~rmccreer/shift.html.
[45] H. G. M. Edwards, E. M. Newton, J. Russ, J. Mol. Struct. **550-551**, 245 (2000).
[46] H. G. M. Edwards, D. W. Farwell, S. J. Rose, D. N. Smith, J. Mol. Struct. **249**, 233 (1991).
[47] J. J. Freeman, A. Wang, K. E. Kuebler, L. A. Huskin, Lunar & Planetary Science XXXIV, Houston, Texas, 2003, Abstract #1676.
[48] L. Burgio, R. J. H. Clark, Spectrochim. Acta Part A **57**, 1491 (2001).
[49] N. Wada, W. A. Kamitakahara, Phys. Rev. B **43**, 2391 (1991).
[50] A. Wang, J. Freeman, K. E. Kuebler, Lunar & Planetary Science XXXIII, Houston, Texas, 2002, Abstract #1374.
[51] C. Rinaudo, M. Roz, V. Boero, M. Franchini-Angela, Neues Jb. Miner. Monat. **12**, 537 (2004).
[52] H. G. M. Edwards, L. Drummond, J. Russ, Spectrochim. Acta **54A,** 1846 (1988).
[53] B. J. Berenblut, P. Dawson, G. R. Wilkinson, Spectrochim. Acta **29A**, 29 (1973).
[54] T. Ohsaka, F. Izumi, Y. Fujiki, J. Raman Spectrosc. **7**, 321 (1978).
[55] E. Murad, Am. Mineral. **82**, 203 (1997).
[56] Y. H. Zhang, C. K. Chan, J. F. Porter, W. Guo, J. Mat. Sci. **13**, 2602 (1998).
[57] Instituto Geológico y Minero de España, Mapa Geológico de España E. 1:50000, Villar del Humo, Servicio de Publicaciones, Ministerio de Industria, 2nd series, 1st ed., Madrid, Spain (1975).
[58] G. Benito, M. J. Machado, C. Sancho, Environ. Geol. **22**, 71 (1993).
[59] J. F. Ruiz, Ph D. Thesis, UNED, Faculty of Geography and History, Madrid, 1996.
[60] E. Doehne in S. Siegesmund, T. Weiss, A. Vollbrecht (eds.) Natural stone, weathering phenomena, conservation strategies and case studies; Geological Society: London, 2002; Special Publications **205**, pp. 55-64.
[61] E. V. Petrova, N. V. Gvozdev, L. N. Rashkovich, J. Optoelectron. Adv. Mater. **6**, 261 (2004).
[62] O. Braissant, Naturwissenschaften **89**, 266 (2002).
[63] N. Sahin, Res. Microbiol. **154**, 399 (2003).

*Corresponding author: ahernanz@ccia.uned.es